Sophia A. Bellia, Lara I. Teodoro, Joseph Traver, Gary L. Guillet, Matthias Zeller and Patrick C. Hillesheim\*

# Structural, surface, and computational analysis of two vitamin-B1 crystals with sulfonimide-based anions

https://doi.org/10.1515/zkri-2021-2040 Received June 21, 2021; accepted September 6, 2021; published online September 20, 2021

Abstract: Two crystals incorporating the thiamine-HCl cation and the fluorinated anion 1,3-disulfonylhexa fluoropropyleneimide have been characterized via singlecrystal X-ray diffraction. The host-guest interactions of thiamine with the anions are analyzed and characterized using Hirshfeld surface analysis. The cations in both structures form a dimer in the solid-state via reciprocal hydrogen bonding through the amine and hydroxyl moieties. Additional investigation into the interactions responsible for dimer formation found that the sulfur atom in the thiazolium ring interacting with several hydrogen atoms to form stabilizing interactions. These interactions in the dimer are further analyzed using reduced density gradient analysis and the results are correlated to the fingerprint plots derived from the Hirshfeld surfaces. Moreover, specific interactions are observed from the cyclical anions, with both the fluorine and sulfonyl oxygen atoms participating in bridging interactions, displaying the diverse host-guest properties of thiamine.

**Keywords:** crystal structure analysis; Hirshfeld surfaces; ionic liquids; RDG analysis; vitamin B1.

## 1 Introduction

Aside from its well-established history as an important nutrient [1], vitamin B1 (or thiamine/thiamin) has also

\*Corresponding author: Patrick C. Hillesheim, Department of Chemistry and Physics, Ave Maria University, Ave Maria, FL 34142, USA; and Department of Chemistry and Physics, Florida Gulf Coast University, Fort Myers, FL 33965, USA,

E-mail: Patrick.Hillesheim@avemaria.edu. https://orcid.org/0000-0002-9567-4002

Sophia A. Bellia, Lara I. Teodoro and Joseph Traver, Department of Chemistry and Physics, Ave Maria University, Ave Maria, FL 34142, USA Gary L. Guillet, Department of Chemistry and Biochemistry, Georgia Southern University, Savannah, GA 31419, USA. https://orcid.org/0000-0002-3696-363X

Matthias Zeller, Department of Chemistry, Purdue University, West Lafayette, IN 47907, USA

found applications across nearly all areas of chemistry including nanoparticle synthesis [2], solid-state materials design [3], as well as having a tremendous impact on rational catalyst design [4-7]. Throughout all of these fields, one of the most important underlying principles of chemistry echoes: structure begets function [8-10]. One of the first reports involving aspects of the structure of vitamin B1 was from Bernal and Crowfoot wherein they discuss the morphology of several crystalline samples of vitamin B1 [11]. The molecular structure of thiamine was acquired from diffraction data reported by Kraut and Reed wherein they discuss the structure of the hydrochloride salt of vitamin B1, first noting the extensive hydrogen bonding present in the compound [12]. The molecular structure reported by Kraut and Reed also showed some of the important characteristic features of vitamin B1. For example, the pyrimidinium ring and the thiazolium ring were found to be orthogonal. Subsequent studies on the structure of thiamine, and other derivatives, were analyzed and it was found that these rings can be found in distinct orientations which were given the labels F, S, or V [13]. The historical definition of these configurations is based on the observed torsion angles  $\varphi_T$  and  $\varphi_P$  corresponding to the torsion angles of C5'-C35'-N3-C2 and N3-C35'-C5'-C4', respectively [14]. The three different configurations (that is F, S, or V) are influenced, in part, by substitutions at the C2 position of the thiazolium ring, Figure 1 [15].

The three structural configurations of thiamine, and its phosphorylated derivatives, affect the host-guest properties of the molecule [16, 17]. As the conformations of thiamine change, several anion binding pockets are formed which are referred to as anion-holes or anion-bridges. Essentially, there exist up to three locations wherein an anion can form interactions that link the pyrimidinium and thiazolium rings through a series of noncovalent interactions (pyrimidinium···anion···thiazolium). These pockets are referred to by the symbols I, II, and III, with each corresponding to a specific set of atoms involved with the bridging interactions [18–21]. The nature, size, and existence of these anion pockets are dependent on the conformations of the rings as well as the local geometry of the ethyl alcohol side-chain (C51–C52–O53–H).

Figure 1: (Left) Thiamine-HCl with labeling scheme used for the structures herein based on previous reports [16] and (right) depiction of the 1,3-disulfonylhexafluoropropyleneimide anion.

Thiamine has tremendous potential in that it is a naturally occurring cation making it a readily available precursor to forming ionic liquids. Ionic liquids (ILs) are a class of materials that are typically comprised of an organic cation with an inorganic anion, with melting points typically below 100 °C [22, 23]. One of the most studied anions used in the development of ILs is bis(trifluoromethanesulfonyl)imide [22, 24]. However, other fluorous anions are capable of forming ILs as well, including the less-studied cyclical anion 1,3-disulfonylhexafluoropropyleneimide or [NCvF]<sup>-</sup> [25, 26]. Due to the cationic nature of thiamine, ILs based on the vitamin B1 structure have previously been reported and studied [27, 28]. ILs incorporating the thiamine cation can be considered as task-specific ionic liquids given the presence of the varied functional groups on the molecule, such as the alcohol and amine moieties, making these cations ideal targets for applications such as catalysis [29–31]. Further, it has been demonstrated that the thiazolium sulfur atom can also be used as a functional group, useful for the polymerization of sterically unhindered monomers [32].

Recently our group has reported on the synthesis and structure of a series of ILs of thiamine paired with perfluorinated anions [33]. In these studies, it was found that the geometry of the anions was useful in facilitating distinct cation ··· cation interactions, with the [NCyF] anion leading to a dimerization of the cations. Herein, we continue our previous studies by reporting two new IL-type structures based on thiamine and [NCyF]<sup>-</sup> anions. Only six examples of crystal structures exist with the [NCyF] anion, making new reports useful for the further development of novel compounds incorporating this anion [33–36]. To assess both short and long-range interactions in the structures, Hirshfeld surface analysis of the structure was performed [37–40]. Surface analysis shows a number of features accounting for the observed interactions in the crystal structures. For example, the specific cation ··· cation interactions in the two structures can be noted by the distinctive shapes seen in the fingerprints of the cations calculated from the Hirshfeld surfaces. We also further investigate the dimeric structure of the cations by using

reduced density gradient analysis to evaluate the intermolecular forces and correlate these findings with the surface analysis, allowing for a more in-depth study of these vitamin-based ionic compounds.

# 2 Materials and methods

#### 2.1 Single crystal growth

Both compounds were synthesized following the established procedure [33]. In brief, thiamine-HCl (1 eq) was dissolved in a minimal amount of water. To this solution, lithium 1,3-disulfonylhexafluoropropyleneimide was added (2.2 eq) and the mixture stirred for 1 h. The mixture was filtered and the resultant white solid was washed with cold water and dried under high vacuum. Single crystals showing the structure of 1 were grown from slow diffusion of hexane into an acetonitrile solution of 1. Single crystals of 2 were grown from slow diffusion of diethyl ether into an ethanol solution of 2.

#### 2.2 Single crystal diffraction

Single crystals for compound 1 were coated in Cargille Type NVH immersion oil and transferred to the goniometer of a Rigaku XtalLAB Mini diffractometer with Mo K $\alpha$  wavelength ( $\lambda$  = 0.70926 Å) and a CCD area detector. Examination and data collection were performed at 170 K. For compound 1 data were collected, reflections were indexed and processed, and the files scaled and corrected for absorption using CRYSALIS PRO [41].

Single crystals of compound **2** were coated with Parabar 10312 oil and transferred to the goniometer of a Bruker D8 Quest Eco diffractometer with Mo K $\alpha$  wavelength ( $\lambda$  = 0.71073 Å) and a Photon II area detector. Examination and data collection were performed at 100 K. Data were collected, reflections were indexed and processed, and the files scaled and corrected for absorption using Apex3 [42], Saint and Sadabs [43].

For all compounds the space groups were assigned using XPREP within the Shelxtl suite of programs [44, 45] and the structures were solved by dual methods using Shellt [46] and refined by full-matrix least-squares against  $F^2$  with all reflections using Shelxl2018 [47] using the graphical interfaces OLEX2 [48] and/or SHELXLE [49]. Carbon bound H atoms were positioned geometrically and constrained to ride on their parent atoms. C-H bond distances were constrained to 0.95 Å for aromatic and alkene C-H moieties, and to 0.99 and 0.98 Å for aliphatic CH<sub>2</sub> and CH<sub>3</sub> moieties, respectively. Alcohol H atoms were positioned geometrically and constrained to ride on their carrying oxygen atoms with O-H distances of 0.84 Å. Methyl and hydroxyl H atoms were allowed to rotate, but not to tip, to best fit the experimental electron density. In 1, amine N-HH atoms were positioned geometrically and constrained to ride on their parent atoms with N-H distances of 0.86 Å. Positions of all other amine hydrogen atoms were refined with N-H distances restrained to target values (0.86(2) or 0.88(2) Å). Water H atom positions were refined and O-H and H···H distances were restrained to 0.84(2) and 1.36(2) Å. Water H atom positions were further restrained based on hydrogen bonding considerations.  $U_{\rm iso}(H)$  values were set to a multiple of  $U_{\rm eq}(C, N \text{ or } O)$  with 1.5 for CH<sub>3</sub> and O-H, and 1.2 for C-H and CH<sub>2</sub>, N-H and NH<sub>2</sub> units, respectively.

In the structure of **2**, one of four crystallographically independent [NCyF]<sup>-</sup> anions is disordered. A diethyl ether molecule was also

refined as disordered. The major and minor [NCvF]- moieties were restrained to have similar geometries, the ether moieties were restrained to have similar geometries as a non-disordered ether molecule in the unit cell (SAME command of Shelxl).  $U_{ii}$  components of ADPs for disordered atoms closer to each other than 2.0 Å were restrained to be similar (SIMU command of Shelxl). Subject to these conditions the occupancy ratio refined to 0.9284(9)-0.0716(9) for the [NCyF] anion and to 0.640(4)-0.360(4) for the ether molecule. A partially occupied water molecule (associated with O54C) induces disorder for one ethylhydroxyl substituent. The major and minor moieties were restrained to have similar geometries (SAME command of Shelxl).  $U_{ii}$  components of ADPs for disordered atoms closer to each other than 2.0 Å were restrained to be similar (SIMU command of Shelxl). The ADPs of methylene C atoms C51B and C51C were constrained to be identical. Subject to these conditions the occupancy ratio refined to 0.926(3)-0.074(3) in favor of the absence of water. Crystallographic data and refinement details for 1 and 2 are given in Table 1.

Complete crystallographic data, in CIF format, have been deposited with the Cambridge Crystallographic Data Centre. CCDC 2090436 and 2090437 contains the supplementary crystallographic data for this paper. These data can be obtained free of charge from The Cambridge Crystallographic Data Centre via www.ccdc.cam.ac.uk/ data\_request/cif.

Crystallographic details are provided in Table 1.

Table 1: Crystallographic data and refinement details for 1 and 2.

Empirical formula	$C_{12}H_{18}N_4OS \cdot C_{12}H_{17}N_4OS \cdot 3(C_3F_6NO_4S_2)$	$C_{12}H_{18}N_4OS\cdot0.019(H_4O_2)$ 2( $C_3F_6NO_4S_2$ )· $C_4H_{10}O$
Formula weight	1408.20	925.47
Crystal system	Monoclinic	Triclinic
Space group	$P2_1/n$	$P\overline{1}$
a/Å	10.1037(3)	13.580(3)
b/Å	21.2709(7)	14.706(4)
c/Å	24.3090(9)	19.425(5)
α/°	90	68.673(8)
β/°	92.281(3)	79.799(7)
γ/°	90	80.771(7)
Volume/ų	5220.2(3)	3537.3(15)
<i>Z</i> / <i>Z</i> ′	4/1	4/2
$D_{\rm c}/{\rm g~cm^{-3}}$	1.792	1.738
F(000)	2848	1881.0
$\mu$ (MoK $\alpha$ )/mm $^{-1}$	0.48	0.451
Measured data	126,275	83,661
θ range for data collection/°	2.2-24.4	2.7–27.9
Unique data	19,593	16,799
R <sub>int</sub>	0.104	0.021
Observed data $(I \ge 2.0 \ \sigma(I))$	9153	14,761
R, obs. data; all data	0.066; 0.166	0.030; 0.037
<ul><li>a, b in weighting</li><li>scheme</li></ul>	0.069; 3.14	0.030, 3.14
$R_w$ obs data; all data	0.149; 0.193	0.073; 0.078
$\Delta  ho_{ m max,min}/{ m e}~{ m \AA}^{-3}$	0.65/-0.47	0.66/-0.53

#### 2.3 Software

Hirshfeld surfaces, images, and two-dimensional fingerprint plots were calculated and produced using CRYSTALEXPLORER17 [50]. Images and analysis of the structures was accomplished using Olex2 [48]. A complete listing of interaction percentages from individual atoms in cations 1A, 1B, 2A, and 2B calculated from the surface analysis is provided in Table 2.

Reduced density gradient (RDG) analysis was accomplished using the MultiWFN software [51]. The wavefunction of the dimer from the crystal structure of 1 was generated using ORCA [52] and NoSpherA2 [53] software suites, employing the B3LYP [54-56] functional, with direct implementation in Olex2. The output files of the RDG analysis from MultiWFN was visualized using gnuplot and VMD [57]. Reduced density gradient isosurface maps (Figure 6) are shown with an isosurface value of 0.65.

# 3 Discussion

With respect to 1, this crystalline sample was a minor component from a slow diffusion of diethyl ether into a saturated solution of the compound in acetonitrile wherein two morphologies of crystal samples were found. The major crystalline sample was reported and discussed in our previous manuscript [33]. Compound 1 crystallizes in the  $P2_1/n$  space group with a dication (labeled A) and a monocation (labeled B) in the asymmetric unit, Figure 2. Three [NCyF] anions present in the asymmetric unit balance the charges from the cations. No solvent or water molecules are present in the structure. Both cations exist in the *F* conformation with  $\varphi_T = 6.8(4)^\circ$  and  $\varphi_P = 93.9(3)^\circ$  for cation **1A**, and  $\varphi_{\rm T} = 10.2(4)^{\circ}$  and  $\varphi_{\rm P} = 84.9(3)^{\circ}$  for cation **1B**. The plane angles for the thiazolium and pyrimidnium rings in cation 1A are 87.60(8)° and the plane angles in 1B are 79.88(9)°.

# 3.1 Compound 1: cation...cation interactions

The two cations are linked through a series of N-H···N, N-H···O and O−H···N hydrogen bonds. The primary hydrogen bond observed in the asymmetric unit is between N1'A-H···N1'B at an H···N distance of 1.939(2) Å, connecting the protonated cationic pyrimidinium nitrogen N1'A of cation 1A with its unprotonated counterpart in cation 1B. The position of the proton is resolved in difference density maps and clearly shifted towards N1'A (the difference density peak is located 0.96 Å from N1'A and 1.83 Å from N1'B), thus confirming the presence of distinct mono and dications in the crystal. Further, this hydrogen-bonding interaction is readily observed on the Hirshfeld surface as the bright red spot over the appropriate nitrogen moieties, indicating an

Table 2: Percentages of interactions arising from atoms for each cation in compounds 1 and 2.

Cation 1A Inside atoms		Outside atoms									
		S	0	Н	N	С	F	Total			
	C	0.2	5.8	0.6	0.2	-	0.1	6.8			
	F	-	_	_	-	-	_	_			
	Н	0.9	27.0	22.8	7.6	0.2	18.2	76.7			
	N	0.5	3.5	2.9	_	_	_	6.8			
	0	-	0.1	2.5	-	-	0.1	2.7			
	S	_	3.2	2.9	0.3	_	0.5	6.9			
	Total	1.7	39.6	31.6	8.1	0.2	18.8				
Cation 1B		Outside atoms									
Inside atoms		S	0	Н	N	С	F	Total			
	C	0.1	2.0	0.2	0.9	-	4.1	7.2			
	F	_	_	_	-	-	_	-			
	Н	0.8	20.4	21.9	4.9	-	26.9	74.8			
	N	0.2	1.1	4.6	0.1	_	3.1	9.2			
	0	-	0.1	2.6	_	_	-	2.7			
	S	0.1	1.1	1.8	0.6	0.1	2.3	6.1			
	Total	1.2	24.7	31.1	6.4	0.1	36.3				
Cation 2A		Outside atoms									
Inside atoms		S	0	Н	N	С	F	Total			
	C	0.1	4.9	1.2	1.0	_	_	7.1			
	F	_	_	_	_	_	_	-			
	Н	1.3	28.9	24.9	5.6	0.1	16.3	77.2			
	N	0.2	2.8	3.3	0.5	_	_	6.8			
	0	_	_	2.5	_	_	_	2.5			
	S	_	3.0	2.9	0.4	_	_	6.3			
	Total	1.6	39.5	35.0	7.5	0.1	16.3				
Cation 2B		Outside atoms									
Inside atoms		S	0	Н	N	С	F	Total			
	C	0.2	5.9	0.6	0.5	_	0.3	7.4			
	F	_	_	_	_	_	_	_			
	Н	0.8	31.1	22.3	7.8	0.5	14.3	76.9			
	N	0.2	3.4	3.3	-	-	-	6.9			
	0	_	0.1	2.5	_	_	_	2.6			
	S	0.1	1.7	2.9	0.5	0.1	0.9	6.2			
	Total	1.3	42.3	31.5	8.8	0.6	15.6				

interaction less than the sum of the van der Waals radii, Figure 3 [37]. Examining the long-range ordering of the cations, there is a distinctive formation of a second form of dimers between the cationic moieties 1A & 1B. Reciprocal hydrogen bonding between the hydroxyl moiety and the pyrimidinium nitrogen (O53–H···N3', d(H···N) = 2.070(2) Å) link the two cations together forming a pocketed dimer in the manner seen in Figure 4. This cation structure was observed in our previous reports of a related structure and appears to be influenced by the geometry of the anion [33]. The alcohol moieties, that is O53A and O53B, also act as hydrogen bond

acceptors, forming close  $H \cdots N$  interactions with the amines (N4'1 and N4'2) at distances ranging 2.0–2.2 Å. These additional O-H···N hydrogen interactions effectively link the dimers into longer chains of discrete dimers. These reciprocal hydrogen interactions are readily seen on the twodimensional fingerprint plots as the sharp spiked features indicated in Figure 5.

Structure 1, as well as 2 (vide infra), exhibits cation···cation interactions leading to the formation of cyclical dimers. To better understand the noncovalent interactions between the two cations leading to the formation of these

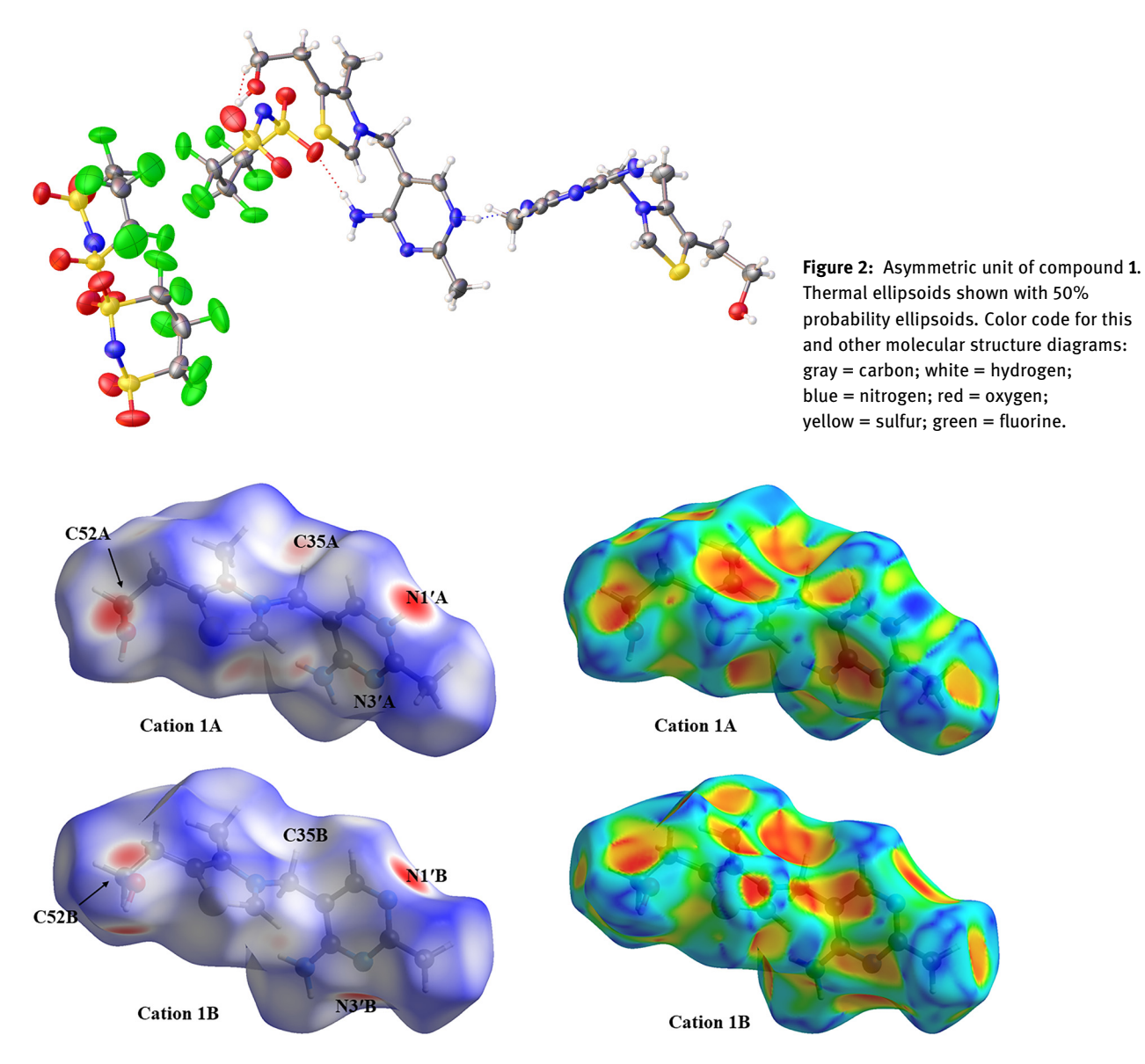


**Figure 3:** The Hirshfeld surfaces for the cations of compound  $\mathbf{1}$  mapped with  $d_{\text{norm}}$  (left) and the shape index (right).

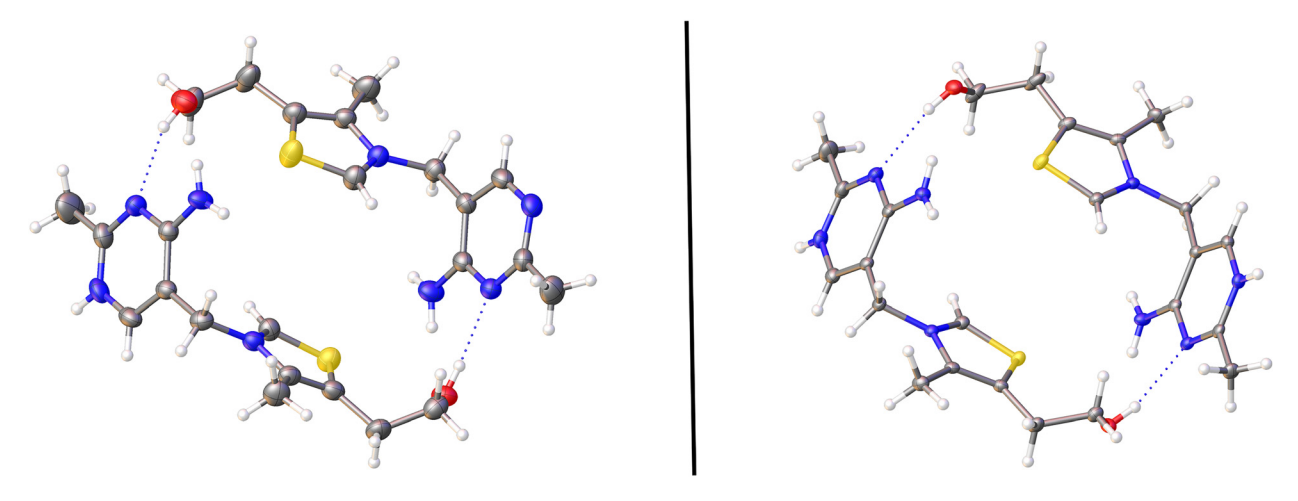
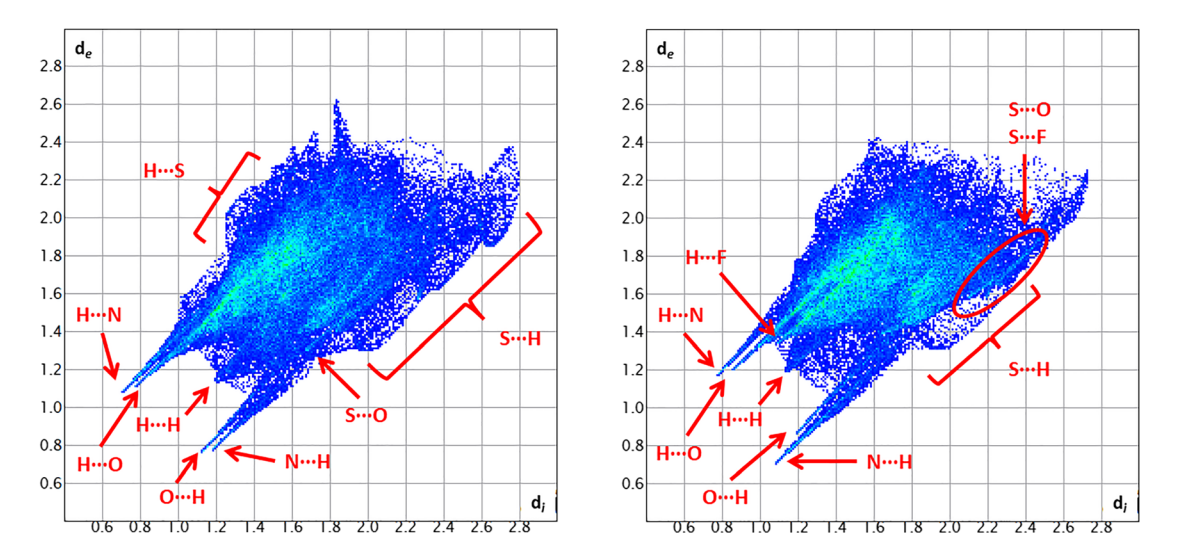


Figure 4: (Left) Cationic dimer formed from reciprocal hydrogen bonding in 1. (Right) The dimer observed in 2, depicting the similarities between the two structures.



**Figure 5:** Two-dimensional fingerprint plots for cation **1A** (left) and **1B** (right). The labeled portions indicate salient structural features observed in the plots.

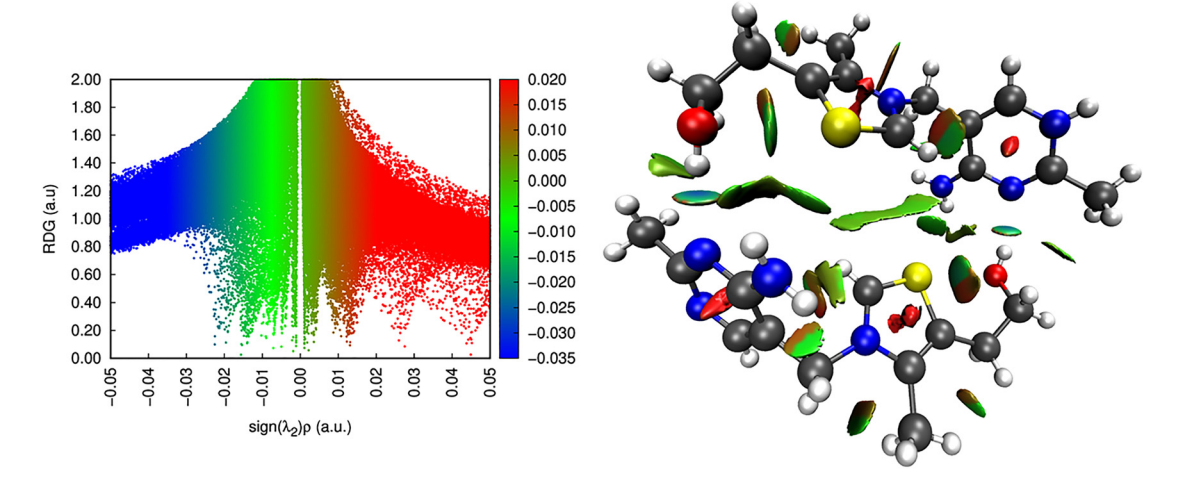


Figure 6: (Left) Scatter plot of the reduced density gradient (RDG) *versus*  $sign(\lambda_2)\rho$ . Coloring is based on the nature of the interactions with blue = attractive interactions (hydrogen bonding), green/tan = van der Waals interactions, red = repulsive interactions (sterics), and (right) RDG isosurface map with an isovalue of 0.65 for the dimeric structure from 1.

dimers, as well as to better recognize the features of the fingerprint plots for the cations, reduced gradient (RDG) analysis was completed on a dimer taken from the structure of 1 [58]. In brief, RDG analysis uses the molecular electron density ( $\rho$ ) and its derivatives to elucidate the types of interactions between atoms allowing for assessment of the relative strength of interactions within a structure or molecule by categorizing the nature of the interaction (hydrogen-bond, van der Waals interaction, steric repulsion) [59, 60]. RDG analysis has been applied to varied systems including crystal structures, protein binding pockets, and ionic compounds of a similar nature to that discussed herein [61, 62]. The scatter plot of  $sign(\lambda_2)\rho$ 

*versus* the RDG and the visualized surface map of these interactions is shown in Figure 6.

Examining the RDG isosurface map (Figure 6) a number of interactions can be can be related to the Hirshfeld surface. For example, the H···S|S···H regions of the fingerprint plots show a disperse, wide ranging set of interactions (Figure 7). Part of these interactions arise from the arrangement of the cations wherein the thiazolium sulfur atoms and the aromatic C2–H moiety interact. While similar sulfur-based interactions have been reported previously to affect long-range supramolecular ordering [63–65], the exact nature and relative contribution to the stabilization or formation of the dimeric structures herein

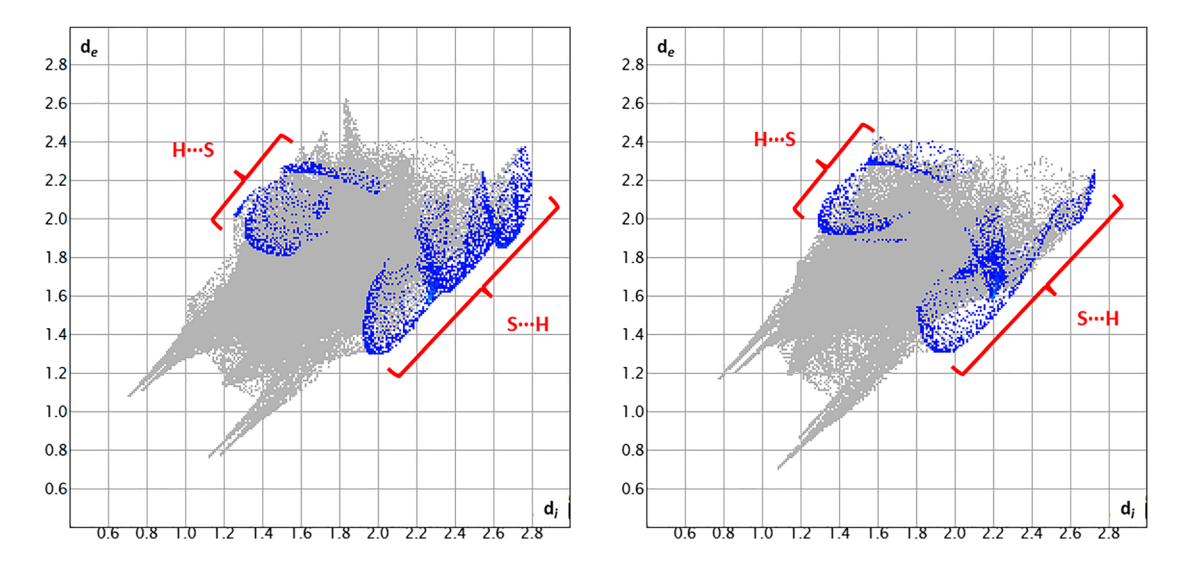


Figure 7: Two-dimensional fingerprints for cations 1A (left) and 1B (right) depicting the H···S|S···H interaction regions.

appears weak given the results of the RDG analysis. However, given the repeated and consistent appearance of these dimers it is plausible that these sulfur interactions do lead to a measure of stabilization given the green coloring  $(\operatorname{sign}(\lambda_2)\rho \approx 0)$ , corresponding to weak, attractive noncovalent interactions.

Other contributions to the  $H \cdots S | S \cdots H$  interactions are seen from the amine moieties (N4'1) on the pyrimidinium rings. The curved surfaces near the amines indicate weak interactions with both the sulfur and the alcohol O53. The geometry of these interactions, however, is such that it is unlikely that these could be considered hydrogen-bonds in the classical sense [66, 67]. Further, the N4'1···O53 distance of 2.860(3) Å lends evidence to this interaction being classified more as a dispersion/electrostatic interaction [66]. Higher level computational work investigating the exact nature of these contributions to the formation of the different cation-cation structures is currently being conducted to help answer these questions. However, it is apparent that there are a number of H...S interactions which are present in the dimeric structure of the cations within both structures reported herein. Results from the RDG analysis clarify the two sets of H atom donors interacting, to some extent, with the thiazolium sulfur accounting for the disperse set of interactions (Figure 7).

#### 3.1.1 Compound 1: anion interactions

Concerning anion---cation interactions, most interactions arise from the sulfonyl oxygen atoms. While weaker interactions from the fluorine atoms link cations and anions, as has been reported previously, the sulfonyl oxygen atoms of the sulfonimide-based anions have a higher negative charge density than the fluorines which would lead towards increased interactions from these moieties [68, 69]. With respect to anion-holes for cation 1A, anion B sits in the anion-hole I, anion A sits in anion-hole II, and anion C sits in anion-hole III. For reference, an image showing both cations 1A and 1B in the dimeric form with the anions in the respective anion-holes is shown in Figure 8.

For cation 1A, anion B bridges the pyrimidinium and thiazolium cation through  $\pi_{Pvr} \cdots O \cdots H - C2$  interactions wherein two sulfonyl oxygens (O1A & O2A) are interacting with the aromatic C2-H moiety at O···H distances of 2.54 and 2.49 Å, respectively. Additionally, O2A interacts with the  $\pi$ -cloud of the pyrimidinium ring at a distance of d = 3.051(3) Å to the ring center. This bridging interaction is seen in the Hirshfeld surface as the bright red indentations over the pyrimidinium ring and the C2-H moiety on the shape index of the molecule, providing a clearer picture of the bridging nature of the anion pocket, Figure 3.

The red indentations on the top of the surface in Figure 3 correspond to the bridging interactions arising from anion C in the anion-hole III location for cation 1A. The three indentations are from interactions with C6-H, S1A, C35'-H, and C41A-H showing that weaker contacts with methylene (C35'-H), methyl (C41-H), and aryl hydrogens (C6-H) are also a part of the binding pocket interactions. This idea is further emphasized with the observed interactions between anion A and the methylene hydrogens on C35'-H in the anion-hole II position. Anion A shows a number of short interactions, bridging the pyrimidinium and thiazolium through interactions originating from the sulfonyl oxygens (O2A and O5A) with the amine N4'1-H and methylene C52A-H groups at distances of 2.16 Å (O2A···H-N4'1) and 2.31 Å (C52–H···O5A) respectively.

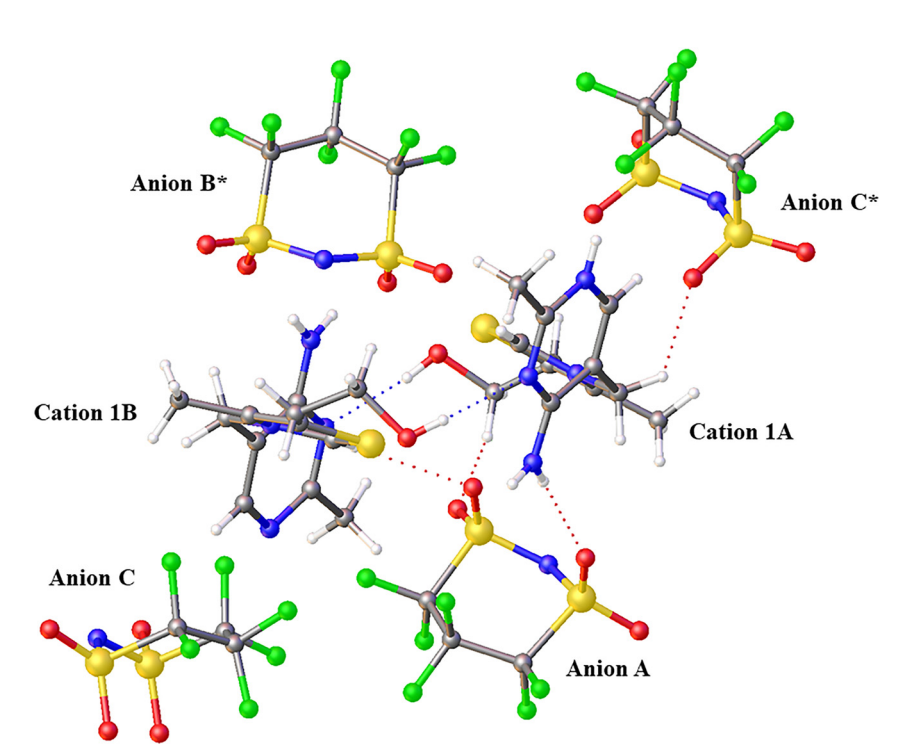


Figure 8: Compound 1 depicted in its dimeric form with the anions residing in the respective anion-holes. The \*indicates the symmetry operator to generate the anion (-1/2 + x, 1/2 - y, 1/2 + z). Atoms depicted as spheres for clarity.

Examining cation 1B, anion A sits in the anion-hole I, anion B in anion-hole II, and anion C in anion-hole III. Some distinct interactions are seen for these bridging interactions when compared to cation 1A. For example, the alignment of anion A is such that the interaction between the anion and the pyrimidinium ring is off-center, with the oxygen aligning above the aromatic carbon C2'B ( $C \cdots O$ , d = 3.238(4) Å) rather than to the ring center. This shifted interaction is readily visualized when examining the mapped  $d_{\text{norm}}$  surface and shape index of the cation (Figure 3). Weaker interactions, noted by the lack of red spots on the mapped  $d_{\text{norm}}$  surface, arise from the shift in the location of the anion while the red curvature over the ring in the shape index is less pronounced and faded. This change in interaction at anion-hole I in 1B is likely due to the electronic structure of the ring as it represents the only neutral pyrimidinium ring in the structures examined herein. Completing the anion-hole I bridging interactions, the S=0···H-C2 (d(0···H) = 2.56 Å) interaction with the central aromatic hydrogen on the thiazolium ring is slightly longer than that in cation 1A.

Anion B, residing in anion-hole II in cation **1B**, displays bifurcated hydrogen bonding with two of the sulfonyl oxygens (O12 & O13) and the amine hydrogens on N4'2-H. The N4'2–H···O12 interaction is shorter ( $d(O \cdot \cdot \cdot H) = 2.470(19) \text{ Å}$ ) compared to the N4'2-H···O13 distance of 2.770(3) Å. Interestingly, there is a notably short interaction with the methyl group C35B and O12 ( $d(O \cdots H) = 2.48 \text{ Å}$ ). Additional  $C-H\cdots O$  interactions between the methylene groups C35B,

C51B, and C52B and the sulfonyl oxygens, ranging from d = 2.7-3.1 Å, complete the bridging interactions between the rings.

Cation 1B shows a distinct set of H...F interactions arising from anion C which sits in the anion-hole III pocket, partially accounting for the more pronounced green spike observed in the fingerprint plot of the cation, Figure 5 [70, 71]. Specifically, two axial fluorine atoms (F1C and F5C) and one equatorial fluorine (F3C) of the anion exhibit the shortest interactions in this location, at distances ranging between 2.76 and 3.22 Å. This is in contrast with the other anion-holes wherein oxygen atoms participate in the shortest interactions. These fluorine interactions are seen when examining the shape index surface, visualized as the three red indentations on the surface over the thiazolium ring. However, it should be noted that the overall shortest H...F interaction in cation 1B is between the methylene C52–H and F3B from anion **B** at d = 2.74 Å.

As has been previously reported regarding the shortrange ordering of ionic liquid-type structures there can be distinct regions of polar, non-polar, and anion/cation clustering [72–75]. Examining the asymmetric unit of 1, the [NCyF]<sup>-</sup> anions are observed in a cluster wherein multiple F...F inter-anionic interactions are observed ranging from ~2.76 to 3.21 Å. Figure 9. A repeating pattern of F...F interactions between anions is seen depicting the fluorous region within the crystal structure. All three of the anions exhibit F···F interactions, with anion B showing the highest percentage (22.2%) followed by anion A (17.0%) and anion C (9.3%). Per the discussion regarding anion-holes (vide supra), the lower percentage of F···F interactions in anion C is due to the arrangement of the fluorine atoms and their use in forming bridging interactions, preventing additional F interactions. These interactions may be stabilizing or destabilizing depending on the distances and angles involved [76, 77]. Examining the interactions depicted in Figure 9, the shortest is d = 2.761(4) Å between F2C···F6A. The angles of this interactions ( $\angle C6C-F2C\cdots F6A = 123.1(3)^{\circ}$ ,  $\angle C8A F6A \cdots F2C = 120.6(2)^{\circ}$ ) are indicative of a type I halogen bond and have been shown to be non-stabilizing interactions [78, 79]. A longer type I interaction between F3A and F4B is also present  $(d = 3.206(5) \text{ Å}, \angle C7B - F4B \cdots F3A = 117.0(3)^{\circ}, \text{ and}$  $\angle$ C7A-F3A···F4B = 120.3(2)°). The remaining interactions with  $d \le 3.2$  Å have angles which do not correspond to established halogen bonding criteria.

## 3.2 Compound 2

Compound 2 crystallizes in the  $P\overline{1}$  space group with two dications and four anions in the asymmetric unit. Figure 10. Two diethyl ether molecules and one partially occupied water molecule are also present in the asymmetric unit. When the water molecule is in the cell, it causes a distinct conformation of the ethyl alcohol chain on the cation, creating disorder in the molecule. Additional disorder in anion C and in the ether molecules are also observed. For the purpose of discussion and surface analysis, only the major portion (~92% occupancy) of the molecules was considered unless otherwise noted. Both of the cations exist in the F conformation of thiamine with  $\varphi_T = 4.69(17)^{\circ}$  and  $\varphi_{\rm P} = 79.98(17)^{\circ}$  for cation **2A**, and  $\varphi_{\rm T} = 5.79(17)^{\circ}$  and

 $\varphi_{\rm P}$  = 80.85(17)° for cation **2B.** The plane angles for the rings are 98.77(5)° for 2A and 103.34(5)° for 2B. One key distinction between 1 and 2 is that both pyrimidine nitrogens, N1'A & N1' B, in 2 are protonated making both moieties dicationic. Four anions in the asymmetric unit balance the charges from the two dications. Figures 11 and 12 depict the two-dimensional fingerprint plots and surfaces for cations 2A and 2B.

To briefly address the impact of the solvent molecules, the H···O hydrogen bonding spike at  $d_i \approx 0.7$  Å,  $d_e \approx 1.1 \text{ Å}$  in the fingerprint of the cation displays shorter contacts when compared to the spikes observed in the fingerprints from **1A** and **1B**. For example, the interactions between the pyrimidinium amine and the oxygen from the ether moiety (N1'A-H···O5',  $d(O \cdot \cdot \cdot H) = 1.825(19) \text{ Å}$ ; N1'B-H···O5B,  $d(O \cdot \cdot \cdot H) = 1.917(15)$  Å) are notably shorter than any H···O hydrogen bonding interactions observed in 1. These shorter interactions are from the protonated pyrimidine nitrogens (N1'A & N1'B) and the ether molecules in the asymmetric unit.

#### 3.2.1 Compound 2: cation...cation interactions

Primary cation...cation interactions are hydrogen bonding through the amine N4'1 and the hydroxyl O53 at a N41-H···O53 distance of 2.081(16) Å. The protonated pyrimidinium nitrogens (N1'A & N1'B) are interacting with solvent molecules, effectively preventing additional cation---cation hydrogen bonding linkages observed in 1. However, similar to that observed in structure 1, the cations in 2 form dimers, held together with the reciprocal hydrogen bonds through O53–H···N3' (d = 2.0969(12) Å). The combination of the solvent molecules occupying hydrogen bonding positions and the formation of the

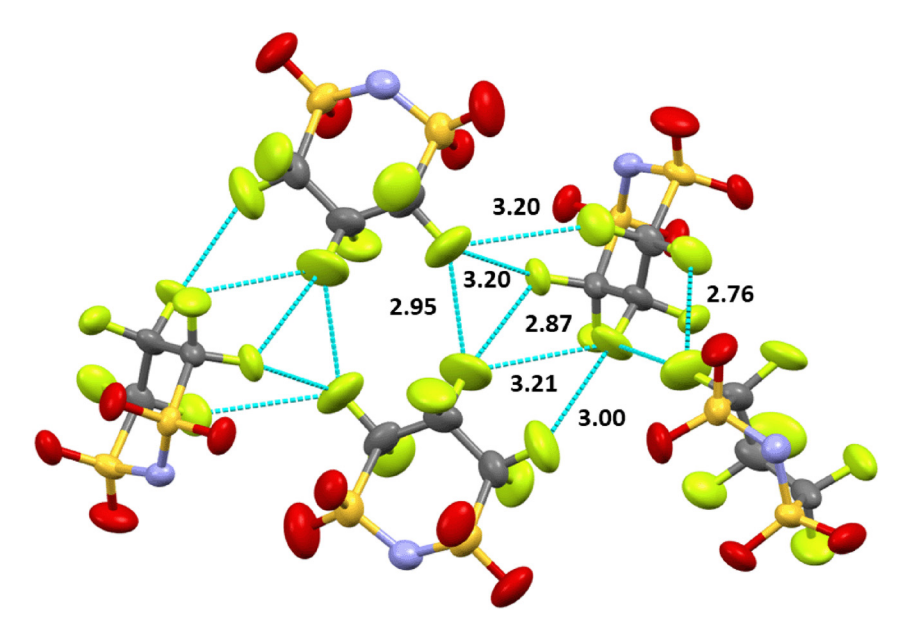
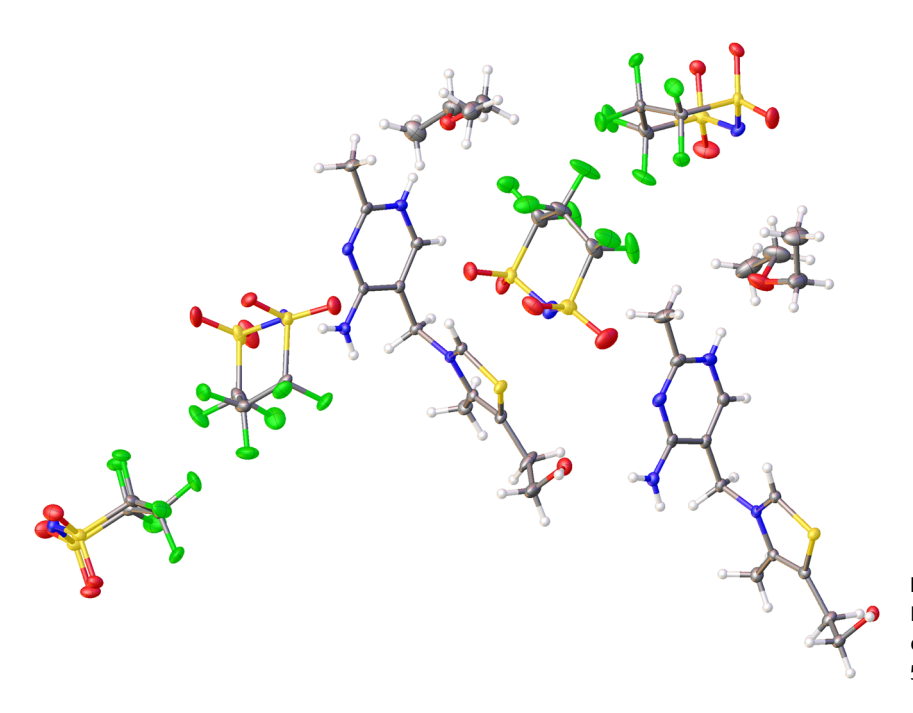


Figure 9: Anions from 1 showing F...F interactions of  $d \le 3.2$  Å. Distances (in Å) are labeled in black with interactions shown in blue.



**Figure 10:** Asymmetric unit of compound **2.** Disordered components are omitted for clarity. Thermal ellipsoids shown at the 50% probability.

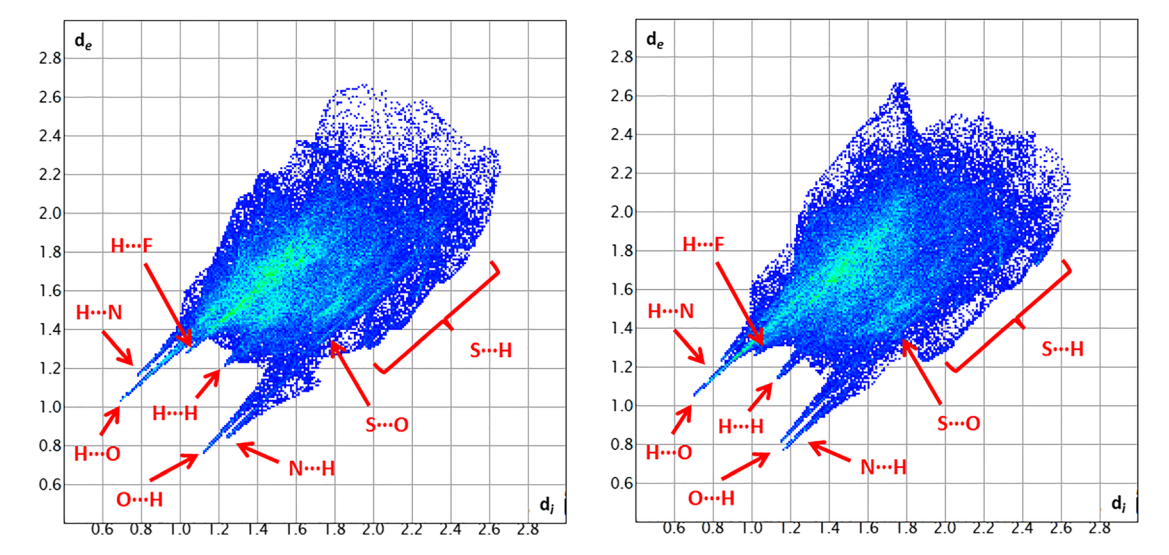


Figure 11: Two-dimensional fingerprint plots for cation 2A (left) and 2B (right). The labeled portions indicate salient structural features observed in the plots.

dimers makes the long-range ordering of the cations nearly identical in both structures, Figure 13.

### 3.2.2 Compound 2: cation...anion interactions

Figure 14 depicts both cations in the dimeric structure with the anions residing in their respective anion-hole locations. For cation **2A**, anions D, B, and C/E (the disordered cation) reside in anion-holes I, II, and III, respectively. Anion D bridges the two heterocyclic rings through the expected  $\pi_{\text{Py}} \cdots O_{\text{SO2}} \cdots H$ –C2 interactions. Both oxygens O4D and O3D participate in a bifurcated hydrogen

interaction with the aromatic C2–H atom at distances of 2.60 and 2.47 Å, respectively. These interactions are similar to those observed in **1A** and **2B**, noted by the disperse set of red interactions seen on the  $d_{\text{norm}}$  mapped surface (Figure 12) of the respective cations in the region around the thiazolium C2–H. Cation **1B** appears unusual in this regard, as the C2–H interaction with the anion appears to only involve a singular oxygen atom as compared with the bifurcated interactions the other three cations exhibit.

As seen in the shape index of cation **2A** (Figure 14), the S= $0 \cdots \pi_{Py}$  interaction is off-center from the pyrimidinium ring, residing instead over the N'1A atom (d = 3.156(2) Å),

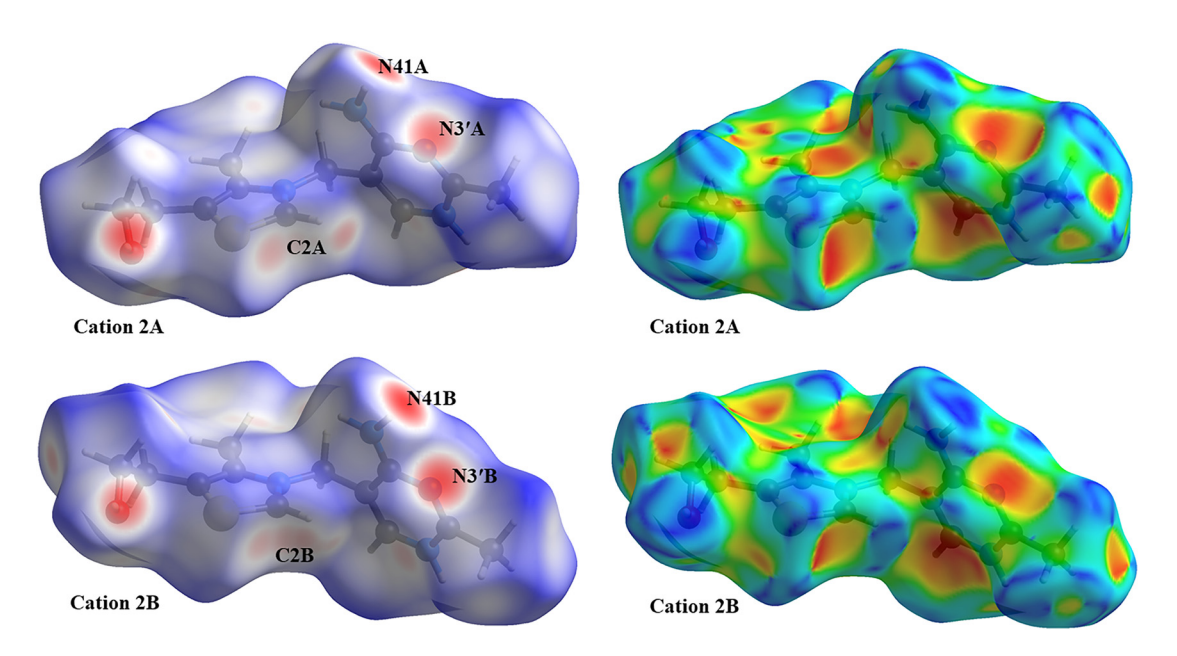


Figure 12: The Hirshfeld surfaces for the cations of compound 2 mapped with  $d_{\text{norm}}$  (left) and the shape index (right).

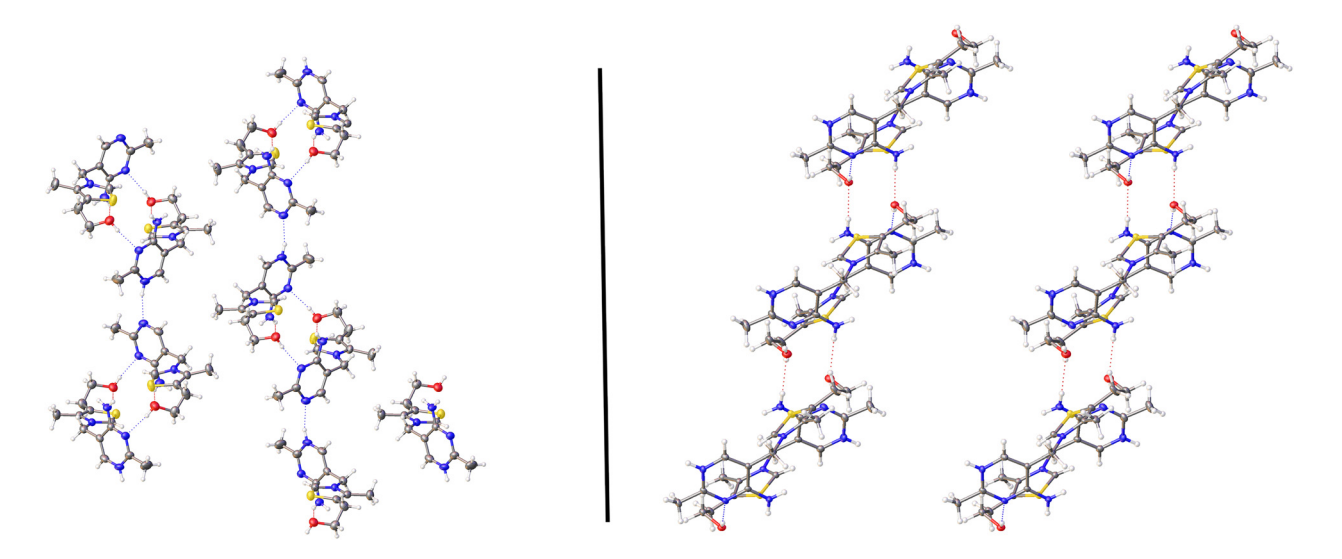
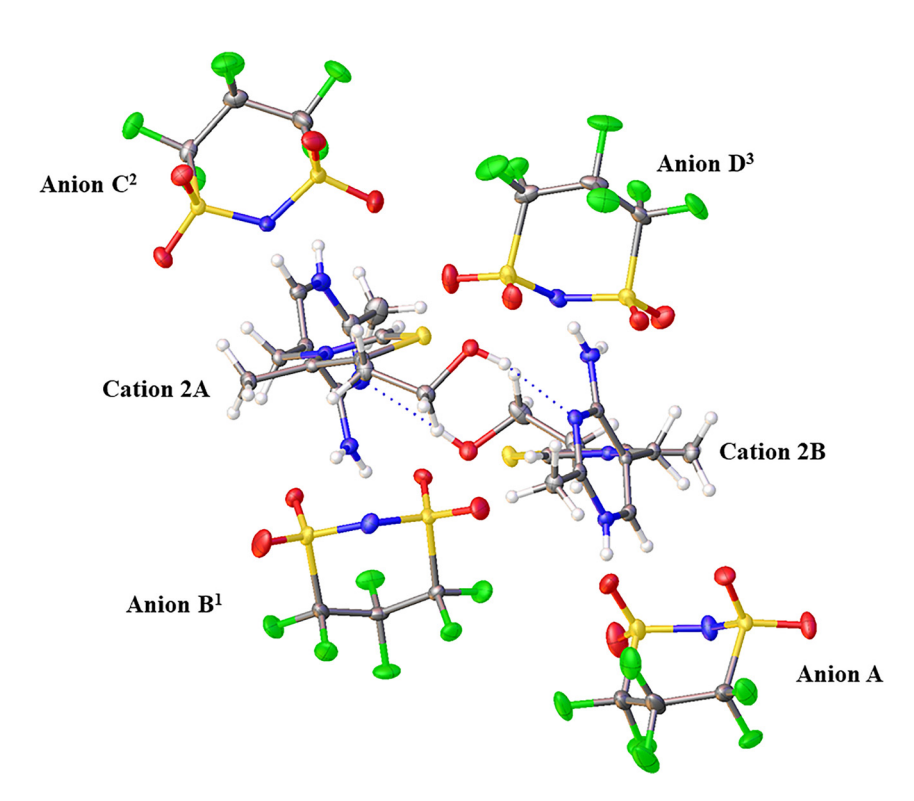


Figure 13: Partial packing diagrams for 1 (left) and 2 (right) viewed from the 100 plane. Hydrogen bonds are shown linking cations together in long-range structure. Anions, solvents, and disorder are omitted for clarity.

likely due to the more positive charge of this protonated amine. However, the presence of the ethyl chains on the solvent molecule could also be shifting the interactions of the anion given the proximity of the alkyl groups with the fluorine atoms of anion D (H···F, with d in the range 2.55–2.91 Å).

Five red indentations on the top of the surface for 2A in the anion-hole II position are from the four sulfonyl oxygen atoms and the imide nitrogen (N5B) from anion B interacting with the thiazolium ring. Both oxygens O2B and O4B are interacting with the amine (N41A) hydrogens at distances of 2.297(19) and 2.620(2) Å, respectively. Additional interactions with the methylene carbon C52-H and O3B (d = 2.63 Å) account for a portion of the bridging interactions between the two heterocyclic moieties. Anion B also forms a bridge between the two cations (that is 2A and **2B**) with a short interaction between F4B and C52B–H at a distance of 2.37 Å. It should be noted that this interaction only exists with the major portion of the disordered hydroxyethyl moiety.

The disordered anion set C (major) & E (minor) reside in the anion-hole III pocket of 2A. The ring-flipped geometry of the two anions appears to be linked with the disorder of the



**Figure 14:** Compound **2** depicted in its dimeric form with the anions residing in the respective anion-holes. The numeric superscripts indicate the symmetry operator to generate the anions; 1 = (2 - x, -y, 1 - z); 2 = (1 + x, +y, +z); 3 = (1 - x, 2 - y, -z).

proximal diethyl ether solvent bound to N1'A as the ethyl chains for the solvent form close contacts with the minor anion E (C16'-H···F5E; d = 2.16 Å). Curiously, anion E (O4E) exhibits the shortest contact with the aromatic hydrogen C6' A-H at a distance of 2.22 Å. The ring flip along with the positional shift of anion C practically eliminates this interaction, in essence removing the defined bridging interaction of this anion-hole position with the C6'A-H aromatic hydrogen [80]. Finally, anion C shows a short interaction with the methylene linker C35A-H and O3C at a distance of 2.66 Å. Further, the imide nitrogen (N5C) is interacting with the cationic aromatic nitrogen N3A (d = 3.1756 (18) Å). While these specific interactions do seem perhaps unusual given the observed pattern of interactions for these complexes, organic molecular packing is often quite complex and the molecules will arrange themselves to maximize interactions and minimize empty space [71].

The cation···anion interactions in **2B** share many similarities with **2A**, perhaps best visualized when contrasting their fingerprint plots (Figure 11). Anion B sits in anion-hole I, D sits in anion-hole II, and A in anion-hole III. As briefly discussed previously, the shape index and mapped  $d_{\text{norm}}$  surface of the two cations help in visualizing the similarities of the interactions of the two moieties. O3B on anion B shows the closest contact with the  $\pi$ -bonding region between N1'B–C2'B at a distance of 2.9510(19) Å. These O··· $\pi$  interactions have been previously reported and studied for their stabilizing influence on protein and other small

molecule structures [81]. Further, as previously mentioned, two sulfonyl oxygen atoms (O3B and O4B) display bifurcated hydrogen interactions with the central aromatic C2B—H at distances of 2.43 and 2.63 Å respectively, completing the expected pyrimidinium…anion…thiazolium bridge.

With respect to the major portion of the disorder, anion D sitting in the anion-hole II position displays the expected interactions between the cation and anion. For example, the bifurcated hydrogen bonding between the amine (N41B) to the sulfonyl oxygen moieties (O2D and O4D) is seen at a N41B–H···O2D distance of 2.310(2) Å and a N41B–H···O4D distance of 2.700(2) Å. Examining the shape index of the cation, one can see the four points of contact in the area above the thiazolium ring, corresponding to the close-contacts of the four sulfonyl oxygen atoms with the  $\pi$ -system of the ring.

Of particular note, with respect to cation **2B**, is an interaction which is only observed in the minor portion of the disorder involving the ethyl alcohol side chain, Figure 15. When the water moiety is present in the cell, this shifts the S1B–C5B–C51B–C52B torsion angle of the sidechain from 30.8(2)° to 101.2(14)°. This shift allows for a notably shorter O53–H···N5D hydrogen bond to form with the imide moiety of anion D sitting in the anion-hole II pocket at a distance of d = 2.0083(14) Å. Of the structures we have reported previously and herein, this is the only example of a direct hydrogen bond with the imide nitrogen of the anion which has been observed.

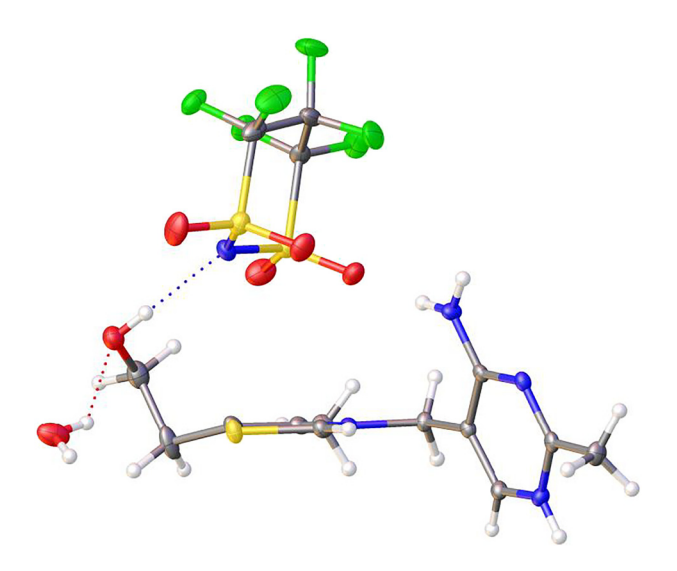


Figure 15: The disordered portion of cation 2B showing the alcohol moiety hydrogen bonding with the imide nitrogen of the anion in the anion-hole II pocket.

Finally, anion A resides in the anion-hole III pocket for cation 2B. O2A makes the shortest interaction with the aromatic C6'B-H moiety at a distance of 2.39 Å O4A then completes the anion bridge with an interaction to the  $\pi$  bond between C2–N3 on the thiazolium ring (d = 2.9157(16) Å).

## 4 Conclusions

Thiamine-based structures continue to show a diverse set of interactions with sulfonimide anions including traditional hydrogen bonding as well as numerous other noncovalent interactions. Multiple orientations of the anions are seen making distinctive interactions to complete the cation---anion---cation bridges which define the anion-hole pockets. The structures presented herein and the inclusion of RDG analysis provides further evidence regarding the ordering of the cations being influenced by anion geometry. The studies herein also continue to add to structural information of the 1,3-disulfonylhexafluoropropyleneimide anion, which remains a rarely studied anion compared to the more popular anions such as trifluoromethanesulfonate or bis(trifluoromethanesulfonyl)imide.

Author contributions: All the authors have accepted responsibility for the entire content of this submitted manuscript and approved submission. Sophia A. Bellia: Methodology, Formal Analysis, Writing - Original Draft, Resources, Investigation. Lara I. Teodoro: Methodology, Investigation. Joseph Traver: Methodology, Investigation.

Gary L. Guillet: Data Curation, Investigation, Writing -Review & Editing, Formal Analysis. Matthias Zeller: Data Curation, Investigation, Writing - Review & Editing, Formal Analysis. Patrick C. Hillesheim: Conceptualization, Methodology, Validation, Visualization, Formal Analysis, Supervision, Project Administration, Writing – Original Draft, Review & Editing.

**Research funding:** This work was supported by Ave Maria University Department of Chemistry and Physics; Parts of this material is based upon work supported by the National Science Foundation through the Major Research Instrumentation Program under Grant Nos. CHE 1530959 and 1919785.

Conflict of interest statement: The authors declare no conflicts of interest regarding this article.

## References

- 1. Manzetti S., Zhang J., van der Spoel D. Thiamin function, metabolism, uptake, and transport. Biochemistry 2014, 53, 821.
- 2. Nadagouda M. N., Polshettiwar V., Varma R. S. Self-assembly of palladium nanoparticles: synthesis of nanobelts, nanoplates and nanotrees using vitamin B1, and their application in carboncarbon coupling reactions. J. Mater. Chem. 2009, 19, 2026.
- 3. Ghafuri H., Joorabchi N., Emami A., Esmaili Zand H. R. Covalent modification of graphene oxide with vitamin B1: preparation, characterization, and catalytic reactivity for synthesis of benzimidazole derivatives. Ind. Eng. Chem. Res. 2017, 56, 6462.
- 4. Chen X.-Y., Gao Z.-H., Ye S. Bifunctional N-heterocyclic carbenes derived from I -pyroglutamic acid and their applications in enantioselective organocatalysis. Acc. Chem. Res. 2020, 53, 690.
- 5. Enders D., Balensiefer T. Nucleophilic carbenes in asymmetric organocatalysis. Acc. Chem. Res. 2004, 37, 534.
- 6. Chhabria M. T., Patel S., Modi P., Pathik S. Brahmkshatriya: thiazole: a review on chemistry, synthesis and therapeutic importance of its derivatives. Curr. Top. Med. Chem. 2016, 16, 2841.
- 7. Kashyap S. J., Garg V. K., Sharma P. K., Kumar N., Dudhe R., Gupta J. K. Thiazoles: having diverse biological activities. Med. Chem. Res. 2012, 21, 2123.
- 8. Beaujuge P. M., Fréchet J. M. Molecular design and ordering effects in  $\pi$ -functional materials for transistor and solar cell applications. J. Am. Chem. Soc. 2011, 21, 20009-20029.
- 9. Desiraju G. R. Crystal engineering: a holistic view. Angew. Chem. Int. Ed. 2007, 46, 8342.
- 10. Trost B. M. Asymmetric catalysis: an enabling science. Proc. Natl. Acad. Sci. USA 2004, 101, 5348.
- 11. Bernal J. D., Crowfoot D. Crystal structure of vitamin B1 and of adenine hydrochloride. Nature 1933, 131, 911.
- 12. Kraut J., Reed H. J. The crystal structure of thiamine hydrochloride (vitamin B). Acta Crystallogr. 1962, 15, 747.
- 13. Pletcher J., Sax M., Blank G., Wood M. Stereochemistry of intermediates in thiamine catalysis. 2. Crystal structure of DL-2-(.alpha.-hydroxybenzyl)thiamine chloride hydrochloride trihydrate. J. Am. Chem. Soc. 1977, 99, 1396.

- 14. Hu N.-H., Norifusa T., Aoki K. Anion coordination and molecular assembly in C2-substituted thiamine-anion systems: effects of the anion and molecular conformation. Dalton Trans. 2003, 3, 335-341.
- 15. Clemente D. A., Marzotto A., Valle G. Crystal and molecular structure of thiamine monochloride. J. Crystallogr. Spectrosc. Res. 1988, 18, 147.
- 16. Hu N.-H., Aoki K., Adevemo A. O., Williams G. N. Host-guest-like thiamine-anion complexation in thiaminium bis(tetrafluoroborate). Acta Crystallogr. C 2001, 57, 1064.
- 17. Hu N.-H., Liu W., Aoki K. Thiamine as a cationic host in anion coordination chemistry. Bull. Chem. Soc. Jpn. 2000, 73, 1043.
- 18. Hu N. H., Zhang S. L. Interactions of thiamine with anions. Structure of thiamine dithiocyanate. Acta Crystallogr. C 1993, 49, 1178.
- 19. Hu N.-H., Liu Y.-S., Aoki K. Interactions of thiamine with anions: (Hthiamine)(thiamine) heptaiododimercurate dihydrate and its dimethanol monohydrate. Acta Crystallogr. C 1999, 55, 304.
- 20. Aoki K., Hu N.-H., Tokuno T., Adeyemo A. O., Williams G. N. Interactions between thiamine and large anions. Crystal structures of (H-thiamine)[PtII(SCN)<sub>4</sub>]·3H<sub>2</sub>O and (H-thiamine) [PtIV(SCN)<sub>6</sub>]·H<sub>2</sub>O. Inorg. Chim. Acta. 1999, 290, 145.
- 21. Archibong E., Adeyemo A., Aoki K., Yamazaki H. Thiamine-metal ion and thiamine-anion interactions. Crystal structure of Cu(thiamine)Br2. Inorg. Chim. Acta 1989, 156, 77.
- 22. MacFarlane D. R., Kar M., Pringle J. M. Fundamentals of Ionic Liquids; Wiley-VCH Verlag GmbH & Co. KGaA: Weinheim, Germany, 2017.
- 23. Abbott A. P., Ryder K., Licence P., Taylor A. W. What is an ionic liquid? In Natalia V. P., Kenneth R. S., Eds. Ionic Liquids Completely UnCOILed; John Wiley & Sons: Hoboken, New Jersey, 2015.
- 24. Golding J. J., MacFarlane D. R., Spiccia L., Golding J. J., Forsyth M., Skelton B. W., White A. H. Weak intermolecular interactions in sulfonamide salts: structure of 1-ethyl-2-methyl-3-benzyl imidazolium bis[(trifluoromethyl)sulfonyl]amide. Chem. Commun. 1998, 1593-1594.
- 25. Siu B., Cassity C. G., Benchea A., Hamby T., Hendrich J., Strickland K. J., Wierzbicki A., Sykora R. E., Salter E. A., O'Brien R. A., West K. N., Davis J. H. Thermally robust: triarylsulfonium ionic liquids stable in air for 90 days at 300 °C. RSC Adv. 2017, 7, 7623.
- 26. Siegel D. J., Anderson G. I., Cyr N., Lambrecht D. S., Zeller M., Hillesheim P. C., Mirjafari A. Molecular design principles of ionic liquids with a sulfonyl fluoride moiety. New J. Chem. 2021, 45, 2443.
- 27. Yang G.-P., Wu X., Yu B., Hu C.-W. Ionic liquid from vitamin B1 analogue and heteropolyacid: a recyclable heterogeneous catalyst for dehydrative coupling in organic carbonate. ACS Sustain. Chem. Eng. 2019, 7, 3727.
- 28. Yang G., Li K., Zeng K., Li Y., Yu T., Liu Y. Heteropolyacid ionic liquid heterogeneously catalyzed synthesis of isochromans via oxa-Pictet-Spengler cyclization in dimethyl carbonate. RSC Adv. 2021, 11, 10610.
- 29. Davis Jr. J. H. Task-specific ionic liquids. Chem. Lett. 2004, 33, 1072.
- 30. Giernoth R. Task-specific ionic liquids. Angew. Chem. Int. Ed. 2010, 49, 2834.
- 31. Visser A. E., Swatloski R. P., Reichert W. M., Davis J. H. Jr., Rogers R. D., Mayton R., Sheff S., Wierzbicki A. Task-specific ionic liquids for the extraction of metal ions from aqueous solutions. Chem. Commun. 2001, 135-136; https://doi.org/10.1039/
- 32. Tian G., Liu W., Chen L., Wu G., Chen S., Wang Y. Thiazolium as single-group bifunctional catalyst for selectively bulk melt ROP of cyclic esters. ChemCatChem 2019, 11, 3388.

- 33. Traver J., Chenard E., Zeller M., Guillet G. L., Lynch W. E., Hillesheim P. C. Directing cation-cation interactions in thiamine compounds: analysis of a series of organic salts based on vitamin B1. J. Mol. Struct. 2021, 1232, 130046.
- 34. Mochida T., Ishida M., Tominaga T., Takahashi K., Sakurai T., Ohta H. Paramagnetic ionic plastic crystals containing the octamethylferrocenium cation: counter anion dependence of phase transitions and crystal structures. Phys. Chem. Chem. Phys. 2018, 20, 3019.
- 35. Moriya M., Watanabe T., Nabeno S., Sakamoto W., Yogo T. Crystal structure and solid-state ionic conductivity of cyclic sulfonylamide salts with cyano-substituted quaternary ammonium cations. Chem. Lett. 2014, 43, 108.
- 36. Mochida T., Funasako Y., Inagaki T., Li M.-J., Asahara K., Kuwahara D. Crystal structures and phase-transition dynamics of cobaltocenium salts with bis(perfluoroalkylsulfonyl)amide anions: remarkable odd-even effect of the fluorocarbon chains in the anion. Chem. Eur J. 2013, 19, 6257.
- 37. Spackman M. A., Jayatilaka D. Hirshfeld surface analysis. CrystEngComm 2009, 11, 19.
- 38. McKinnon J. J., Mitchell A. S., Spackman M. A. Hirshfeld surfaces: a new tool for visualising and exploring molecular crystals. Chem. Eur J. 1998, 4, 2136.
- 39. Spackman M. A., McKinnon J. J. Fingerprinting intermolecular interactions in molecular crystals. CrystEngComm 2002, 4, 378.
- 40. McKinnon J. J., Spackman M. A., Mitchell A. S. Novel tools for visualizing and exploring intermolecular interactions in molecular crystals. Acta Crystallogr. B 2004, 60, 627.
- 41. CRYSALIS PRO. Oxford Diffraction/Agilent Technologies UK Ltd.: Yarnton, England.
- 42. APEX3 v2019.1-0. SAINT V8.40A. Bruker AXS Inc.: Madison (WI), USA 2019.
- 43. Krause L., Herbst-Irmer R., Sheldrick G. M., Stalke D. Comparison of silver and molybdenum microfocus X-ray sources for single-crystal structure determination. J. Appl. Crystallogr. 2015, 48, 3.
- 44. SHELXTL. Suite of Programs, Version 6.14, 2000–2003, Bruker Advanced X-Ray Solutions. Bruker AXS Inc.: Madison (WI), USA.
- 45. Sheldrick, G. M. A short history of Shelx. Acta Crystallogr. A 2008,
- 46. Sheldrick G. M. SHELXT integrated space-group and crystalstructure determination. Acta Crystallogr. Sect. Found. Adv. 2015, 71, 3.
- 47. Sheldrick, G. M. Crystal structure refinement with SHELXL. Acta Crystallogr. Sect. C Struct. Chem. 2015, 71, 3.
- 48. Dolomanov O. V., Bourhis L. J., Gildea R. J., Howard J. A. K., Puschmann H. OLEX2: a complete structure solution, refinement and analysis program. J. Appl. Crystallogr. 2009, 42, 339.
- 49. Hübschle, C. B., Sheldrick, G. M., Dittrich, B. SHELXLE: a Qt graphical user interface for SHELXL. J. Appl. Crystallogr. 2011, 44,
- 50. Turner M. J., McKinnon J. J., Wolff S. K., Grimwood D. J., Spackman P. R., Jayatilaka D., Spackman M. A. CRYSTAL EXPLORER 17; University of Western Australia, 2017.
- 51. Lu T., Chen F. Multiwfn: a multifunctional wavefunction analyzer. J. Comput. Chem. 2012, 33, 580.
- 52. Neese F. Software update: the ORCA program system, version 4.0. WIREs Comput. Mol. Sci. 2018, 8, e1327.
- 53. Kleemiss F., Dolomanov O. V., Bodensteiner M., Peyerimhoff N., Midgley L., Bourhis L. J., Genoni A., Malaspina L. A., Jayatilaka D.,

- Spencer J. L., White F., Grundkötter-Stock B., Steinhauer S., Lentz D., Puschmann H., Grabowsky S. Accurate crystal structures and chemical properties from NoSpherA2. Chem. Sci. 2021, 12, 1675.
- 54. Stephens P. J., Devlin F. J., Chabalowski C. F., Frisch M. J. Ab initio calculation of vibrational absorption and circular dichroism spectra using density functional force fields. J. Phys. Chem. 1994, 98, 11623.
- 55. Becke A. D. A new mixing of Hartree-Fock and local densityfunctional theories. J. Chem. Phys. 1993, 98, 1372.
- 56. Becke A. D. Density-functional thermochemistry. III. The role of exact exchange. J. Chem. Phys. 1993, 98, 5648.
- 57. Humphrey W., Dalke A., Schulten K. VMD: visual molecular dynamics. J. Mol. Graph. 1996, 14, 33.
- 58. Tan S. L., Jotani M. M., Tiekink E. R. T. Utilizing Hirshfeld surface calculations, non-covalent interaction (NCI) plots and the calculation of interaction energies in the analysis of molecular packing. Acta Crystallogr. Sect. E Crystallogr. Commun. 2019, 75, 308.
- 59. Contreras-García J., Johnson E. R., Keinan S., Chaudret R., Piquemal J.-P., Beratan D. N., Yang W. NCIPLOT: a program for plotting noncovalent interaction regions. J. Chem. Theor. Comput. 2011, 7, 625.
- 60. Johnson E. R., Keinan S., Mori-Sánchez P., Contreras-García J., Cohen A. J., Yang W. Revealing noncovalent interactions. J. Am. Chem. Soc. 2010, 132, 6498.
- 61. Saleh G., Gatti C., Lo Presti L., Contreras-García J. Revealing noncovalent interactions in molecular crystals through their experimental electron densities. Chem. Eur. J. 2012, 18, 15523.
- 62. Joseph A., Thomas V. I., Żyła G., Padmanabhan A. S., Mathew S. Theoretical probing of weak anion-cation interactions in certain pyridinium-based ionic liquid ion pairs and the application of molecular electrostatic potential in their ionic crystal density determination: a comparative study using density functional approach. J. Phys. Chem. A. 2018, 122, 328.
- 63. Beno B. R., Yeung K.-S., Bartberger M. D., Pennington L. D., Meanwell N. A. A survey of the role of noncovalent sulfur interactions in drug design. J. Med. Chem. 2015, 58, 4383.
- 64. van Bergen L. A. H., Alonso M., Palló A., Nilsson L., De Proft F., Messens J. Revisiting sulfur H-bonds in proteins: the example of peroxiredoxin AhpE. Sci. Rep. 2016, 6, 30369.
- 65. Zhou P., Tian F., Lv F., Shang Z. Geometric characteristics of hydrogen bonds involving sulfur atoms in proteins. Proteins Struct. Funct. Bioinform. 2009, 76, 151.
- 66. Steiner T. The hydrogen bond in the solid state. Angew. Chem. Int. Ed. 2002, 41, 48.
- 67. Bernstein J., Davis R. E., Shimoni L., Chang N.-L. Patterns in hydrogen bonding: functionality and graph set analysis in crystals. Angew. Chem. Int. Ed. Engl. 1995, 34, 1555.

- 68. Dean P. M., Pringle J. M., Forsyth C. M., Scott J. L., MacFarlane D. R. Interactions in bisamide ionic liquids—insights from a Hirshfeld surface analysis of their crystalline states. New J. Chem. 2008, 32, 2121.
- 69. Logotheti G., Ramos J., Economou I. G. Molecular modeling of imidazolium-based [tf<sub>2</sub>N<sup>-</sup>] ionic liquids: microscopic structure, thermodynamic and dynamic properties, and segmental dynamics. J. Phys. Chem. B 2009, 113, 7211.
- 70. Dunitz J. D. Organic fluorine: odd man out. ChemBioChem 2004, 5, 614.
- 71. Dunitz J. D., Gavezzotti A. How molecules stick together in organic crystals: weak intermolecular interactions. Chem. Soc. Rev. 2009,
- 72. Dupont J. On the solid, liquid and solution structural organization of imidazolium ionic liquids. J. Braz. Chem. Soc. 2004, 15, 341.
- 73. Hayes R., Warr G. G., Atkin R. Structure and nanostructure in ionic liquids. Chem. Rev. 2015, 115, 6357.
- 74. Brehm M., Weber H., Thomas M., Hollóczki O., Kirchner B. Domain analysis in nanostructured liquids: a post-molecular dynamics study at the example of ionic liquids. ChemPhysChem 2015, 16, 3271.
- 75. Canongia Lopes J. N. A., Pádua A. A. H. Nanostructural organization in ionic liquids. J. Phys. Chem. B 2006, 110, 3330.
- 76. Reichenbächer K., Süss H. I., Hulliger J. Fluorine in crystal engineering-"the little atom that could". Chem. Soc. Rev. 2005,
- 77. Eskandari K., Lesani M. Does fluorine participate in halogen bonding? Chem. Eur. J. 2015, 21, 4739.
- 78. Siram R. B. K., Karothu D. P., Guru Row T. N., Patil S. Unique type II Halogen...Halogen interactions in pentafluorophenyl-appended 2,2'-bithiazoles. Cryst. Growth Des. 2013, 13, 1045.
- 79. Cavallo G., Metrangolo P., Milani R., Pilati T., Priimagi A., Resnati G., Terraneo G. The halogen bond. Chem. Rev. 2016, 116, 2478.
- 80. Hu N.-H., Aoki K., Adeyemo A. O., Williams G. N. Metal ion and anion coordination in the thiamine- $[PtII(NO_2)_4]^{2-}$  system. Structures of a metal complex, Pt(thiamine)(NO<sub>2</sub>)<sub>3</sub>, and two salts, (H-thiamine)[Pt(NO<sub>2</sub>)<sub>4</sub>]·2H<sub>2</sub>O and (thiamine monophosphate)2 [Pt(NO<sub>2</sub>)<sub>4</sub>]·2H<sub>2</sub>O. Inorg. Chim. Acta 2001, 325, 9.
- 81. Jain A., Purohit C. S., Verma S., Sankararamakrishnan R. Close contacts between carbonyl oxygen atoms and aromatic centers in protein structures:  $\pi \cdots \pi$  or lone-pair $\cdots \pi$  interactions? *J. Phys.* Chem. B 2007, 111, 8680.

Supplementary Material: The online version of this article offers supplementary material (https://doi.org/10.1515/zkri-2021-2040).